Carbohydrate Polymers 127 (2015) 291–299

Contents lists available at ScienceDirect

Carbohydrate Polymers

journal homepage: www.elsevier.com/locate/carbpol

Improving the physical properties of starch using a new kind of water dispersible nano-hybrid reinforcement

Noé J. Morales[a,b], Roberto Candal[a,c], Lucía Famá[b], Silvia Goyanes[b], Gerardo H. Rubiolo[b,d,*]

[a] Instituto de Química Inorgánica, Medio Ambiente y Energía (INQUIMAE), CONICET – UBA , Ciudad Universitaria, C1428EHA, Buenos Aires, Argentina
[b] Laboratorio de Polímeros y Materiales Compuestos, Departamento de Física, FCEyN, UBA – IFIBA – CONICET, Ciudad Universitaria, C1428EHA, Buenos Aires, Argentina
[c] Instituto de Investigación e Ingeniería Ambiental, Universidad Nacional de San Martín, Campus Miguelete, 25 de Mayo y Francia, 1650 San Martín, Provincia de Buenos Aires, Argentina
[d] Gerencia Materiales, Comisión Nacional de Energía Atómica, Avda Gral Paz 1499, B1650KNA, San Martín, Argentina

ARTICLE INFO

Article history:
Received 31 October 2014
Received in revised form 17 March 2015
Accepted 18 March 2015
Available online 28 March 2015

Keywords:
Cassava starch
Hybrid nanomaterial
Polymer nanocomposite
Carbon nanotubes

ABSTRACT

Plasticized cassava starch matrix composites reinforced by a multi-wall carbon nanotube (MWCNT)–hercynite ($FeAl_2O_4$) nanomaterial were developed. The hybrid nanomaterial consists of $FeAl_2O_4$ nanoparticles anchored strongly to the surface of the MWCNT. This nano-hybrid filler shows an irregular geometry, which provides a strong mechanical interlocking with the matrix, and excellent stability in water, ensuring a good dispersion in the starch matrix. The composite containing 0.04 wt.% of the nano-hybrid filler displays increments of 370% in the Young's modulus, 138% in tensile strength and 350% in tensile toughness and a 70% decrease in water vapor permeability relative to the matrix material. All of these significant improvements are explained in terms of the nano-hybrid filler homogenous dispersion and its high affinity with both plasticizers, glycerol and water, which induces crystallization without deterioration of the tensile toughness.

1. Introduction

In the last decades, there has been a notable increasing interest in the development of plastics from polysaccharides as an alternative to replace synthetic plastic films. The properties of these materials and their potential applications, depend on the type and concentration of the plasticizers and the presence of other additives such as sugars, lipids, etc. (Antoniou, Liu, Majeed, Qazi, & Zhong, 2014; Kalichevsky & Blanshard, 1992; Kalichevsky, Jaroszkiewicz, Ablett, Blanshard, & Lillford, 1992; Nuanmano, Prodpran, & Benjakul, 2015).

Starch is an abundant low cost biopolymer which can be processed to biodegradable films. Water and glycerol are two of the most typical plasticizers used in the production of the processed films (García, Famá, Dufresne, Aranguren, & Goyanes, 2009; Schmitt, Prashantha, Soulestin, Lacrampe, & Krawczak, 2012; Swain, Pradhan, & Sahu, 2013). The structure of starch–glycerol–water films is complex due to the partial miscibility of glycerol in starch (Forssell, Mikkilä, Moates, & Parker, 1997; Wilhelm, Sierakowski, Souza, & Wypych, 2003). These systems can exhibit one or two phases depending on the mass fraction of each component (water, glycerol, starch) (Godbillot, Dole, Joly, Rogé, & Mathlouthi, 2006). According to Moates, Noel, Parker, and Ring (2001), when phase separation takes place, one of the phases is rich in glycerol and the other in starch.

Starch retrogradation may occur during the storage of starch based systems, leading to an incipient crystallization and the consequent modification of the films' mechanical properties. The nature and proportion of the different phases present in the films affect the crystallization process (Farahnaky, Saberi, & Majzoobi, 2013; Farhat, Blanshard, & Mitchell, 2000).

In spite of its multiple advantages, the use of starch based film is still limited because of its poor mechanical properties and high water vapor permeability, compared to other non-natural polymers (Carvalho, 2011; Famá, Rojo, Bernal, & Goyanes, 2012; García, Ribba, Dufresne, Aranguren, & Goyanes, 2011; Hansen & Plackett, 2008). The incorporation of micro and nano-sized fillers into starch matrices has been the topic of many studies in order to overcome

* Corresponding author at: Gerencia Materiales, Comisión Nacional de Energía Atómica, Avda Gral Paz 1499, B1650KNA, San Martín, Argentina.
Tel.: +54 11 6772 7240; fax: +54 11 6772 7362.
E-mail address: rubiolo@cnea.gov.ar (G.H. Rubiolo).

http://dx.doi.org/10.1016/j.carbpol.2015.03.071
0144-8617/

these limitations (Chang, Wu, Anderson, & Ma, 2012; Famá, Pettarin, Goyanes, & Bernal, 2011; Nafchi, Alias, Mahmud, & Robal, 2012).

Inorganic nanoparticles, especially ceramic oxide and nanoclays, were used as fillers with some success in the reinforcement of starch matrices. Multi-wall carbon nanotubes (MWCNTs) have extraordinary mechanical properties that make them outstanding materials to blend with polymers in order to prepare multifunctional nanocomposites (Kong, Yuan, & Qiu, 2012; Sun, Chu, & Sue, 2010; Zilli et al., 2007). However, the effective utilization of nanofillers in composite materials strongly depends on their homogeneous dispersion through the polymer matrix and their adequate interfacial adhesion (Kong et al., 2012; Sun et al., 2010; Zilli et al., 2007).

Carbon nanotubes are strongly affected by van der Waals forces, so, they tend to agglomerate during polymer nanocomposites preparation (Kudus, Akil, Mohamad, & Loon, 2011; Tian & He, 2011). Covalent and non-covalent functionalization as well as the use of surfactants are common ways to disperse MWCNTs in starch. However, functionalization of the nanofiller normally involves a number of steps and is expensive. Besides, covalent functionalization introduces defects and can have a negative effect on MWCNT properties (Escobar et al., 2009; Goyanes et al., 2007).

The synergy between different fillers (like grapheme and nanodiamond or nanodiamond and carbon nanotubes) in the improvement of mechanical properties of polymer plastics was reported (Prasad, Das, Maitra, Ramamurty, & Rao, 2009). Micro sized alumina particles associated with MWCNTs were successfully used as filler for the reinforcement of high density polyethylene. This type of filler shows high dispersibility in the solvent used to prepare the polyethylene composite, leading to a material with better mechanical properties than the composite prepared with only MWCNTs (Tian & He, 2011).

Our research group had recently developed a new nano-hybrid filler composed of ceramic nanoparticles physically anchored to MWCNTs. Notably, this hybrid is easily dispersed in water, produce very stable aqueous suspensions and avoids chemical functionalization or surfactant incorporation (Morales Mendoza et al., 2012; Morales et al., 2013). It should be noted that pristine MWCNTs do not form stable aqueous suspensions without the addition of surfactants and cannot be homogeneously dispersed in suspensions based on starch and water.

The aim of this work is to develop a new starch composite using as reinforcement a water dispersible nano-hybrid filler composed of ceramic nanoparticles attached to carbon nanotube walls. As far as we know, this type of hybrid or others with similar characteristics has not been used to reinforce starch polymers before. The effects of hybrid content on morphological, thermal and structural characteristics of the films, as well as its water vapor permeability and mechanical properties are discussed.

2. Experimental

2.1. Materials

Cassava starch, provided by Industrias del Maíz S.A. (Argentina) with a 28 wt.% amylose and 72 wt.% amylopectin was employed. Glycerol (Mallinckrodt, Argentina) was used as plasticizer. Nanocyl NC 3100 was used as received to prepare a composite containing only carbon nanotubes.

2.2. Nano-hybrid filler preparation

Nano-hybrid filler (NHF) was synthesized as reported in Morales Mendoza et al. (2012). Briefly, the NHF was prepared by chemical vapor deposition (CVD) using α-Fe embedded in hercynite microparticles as a catalyst and acetylene as the carbon source. The catalyst was prepared by a sol–gel method using aluminum sec-butoxide and $Fe(NO_3)_3{\cdot}9H_2O$ as precursors, dissolved in an ethanol/water solution. The hydrolysis and condensation of the precursors were catalyzed by HF acid, leading to a sol formed by particles containing intimately mixed aluminum and iron hydrous-oxides. The drying of the sol under a controlled atmosphere produced first a gel and later a xerogel. The xerogel was fired at 450 °C under air atmosphere, milled in an agata mortar and sieved through stainless steel mesh, (200–350 mesh ASTM) producing the precursor of the catalyst. This precursor was reduced during 2 h at 730 °C under N_2/H_2 atmosphere in a cylindrical oven, leading to the production of micrometric hercynite particles containing embedded α-Fe nanoparticles. Carbon nanotubes were synthesized by introduction of N_2/H_2 plus acetylene in the oven at the same temperature for 1 h. During CNT growing the catalyst particles were exposed to intense stress that produced its fracture in small nanoparticles which remained physically attached to the external walls of the CNTs. The composition of the NHF is 80% carbon nanotubes (MWCNTs) and 20% ceramic components (mostly hercynite ($FeAl_2O_4$) and other minor components). Fig. 1a shows an image of the NHF obtained by Field Emission Scanning Electron Microscopy (FE-SEM). The MWCNTs average outer diameter was 35 nm and the nanoparticles (NP) average size was 50 nm. This NHF is highly dispersible in deionized water producing stable water dispersions, as a consequence of its relatively low isoelectric point (3.2) (Morales et al., 2013). Under the same conditions commercial carbon nanotubes with similar morphological characteristics agglomerate and precipitate after a short time in suspension, as can be seen in Fig. 1b–d.

2.3. Preparation of starch/MWCNT–hercynite hybrid composites

The nanocomposites films were prepared following a similar protocol to that reported in Famá et al. (2011, 2012). The adequate quantity of NHF without further treatment was dispersed in

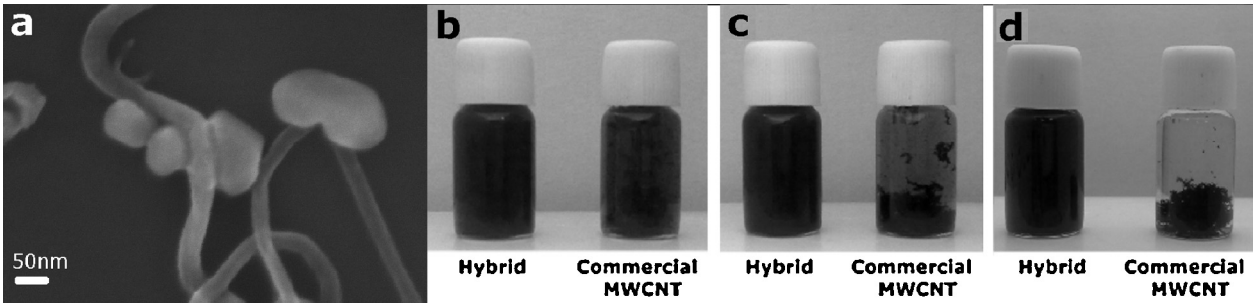

Fig. 1. (a) FE-SEM micrograph of nano-hybrid filler composed by MWCNT and hercynite nanoparticle. Water dispersion of nanofillers: (b) immediately after sonication, (c) after 1 h and (d) 24 days.

93.5 mL of distilled water using a tip sonicator (JY92-IIDN Ningbo Scientz Biotechnology CO) over a period lasting 30 min. Then 1.5 g of glycerol and 5 g of starch were added. The mixture was smoothly stirred for 45 min and was then heated at 3 °C/min until it reached 85 °C. This process guarantees complete gelatinization, as determined by the loss of birefringence. Finally, the gel was degassed with a vacuum pump for 10 min, cast in glass Petri dishes and dried at 50 °C for 24 h. Starch glycerol matrix and composites containing 0.02, 0.04, 0.10 wt.% of MWCNT–hercynite hybrid were developed and identified as matrix, NHF-0.02, NHF-0.04 and NHF-0.10, respectively. The amount of nanofiller added is expressed in percentage weight ratio (wt.%) to the mass of starch and glycerol in the formulation. Since the structure and therefore the properties of these materials are strongly related to the water content, the moisture content of the nanocomposite films was achieved by conditioning the samples for four weeks in desiccators containing NaBr (RH = 57.5% at 25 °C).

Table 1 provides the composition of the samples on dry basis and after conditioning.

2.4. Characterization techniques

2.4.1. Morphological characterization

The morphological characterization of the materials was performed on both macroscopic and microscopic scales.

The presence of agglomerates in the films was studied by optical observations using an Olympus BX60M microscope in the bright field mode. The cryogenic fracture surfaces of the composites were observed by scanning electron microscopy using a FE-SEM with Field Emission Gun (FEG) Zeiss DSM982 GEMINI. The fracture surface of the samples was sputter-coated with gold (15 s, 0.06 mbar of Ar) and observed with an acceleration voltage of 5 kV.

2.4.2. Thermal characterization

Thermo-mechanical determination of the glass transition temperatures (T_g) was carried out in a dynamic mechanical thermal analyzer (DMTA IV, Rheometric Scientific), in the rectangular tension mode at1 Hz and a heating rate of 2 °C/min. The temperature range of measurements was from −100 °C to 75 °C. The strain amplitude was 0.04% to assure that the mechanical response of the samples was within the linear viscoelastic range. Samples dimensions were 15.0 mm × 5.0 mm × 0.26 mm (length, width and thickness, respectively). Three replicates were tested for each system.

The thermal stability of the samples was measured with a thermogravimetric analyzer (Shimadzu TGA-51). Approximately 10 mg of each sample was subjected to heating from 30 to 500 °C at a rate of 10 °C/min in a dry nitrogen atmosphere. The flow rate of nitrogen was 50 mL/min. The mass of the sample was continuously recorded while the sample temperature was ramped at a constant heating rate, then the weight loss as function of the temperature was calculated.

Table 1
Matrix and composite composition on dry basis and on conditioned films.

	Dry basis (wt.%)	Conditioned films (wt.%)
Starch	76.9	67.7
Glycerol	23.1	20.3
Water	–	12**
Filler	0.02/0.04/0.10*	0.018/0.036/0.088***

* Calculated with respect 100% of dry basis matrix.
** Determined by thermogravimetric analysis.
*** Calculated with respect 100% of conditioned matrix.

2.4.3. X-ray diffraction (XRD)

The X-ray diffraction patterns were measured with a Siemens D 5000 X-ray diffractometer. The X-ray generator tension and current were 40 kV and 30 mA, respectively. The radiation was Cu $K\alpha$ of wavelength 1.54 Å. Data were collected in the range $2\theta = 5–35°$ with a step size of 0.02°.

2.4.4. Water vapor permeability (WVP)

Water vapor permeability of composites was determined at room temperature using a modified ASTM E96-00 procedure (Famá et al., 2012). Samples were placed into circular acrylic cells containing $CaCl_2$, and were then located in desiccators at relative humidity (RH) of ~70% and room temperature. Water vapor transport (WVT) through the samples and adsorbed by the desiccant, was determined from the weight gain of the acrylic cells. The cells were weighed daily over 10 days with an accuracy of 0.1 mg. WVP were then calculated as:

$$\mathrm{WVP} = \frac{\mathrm{WVT} \cdot e}{P_0 \cdot \mathrm{RH}} \quad (1)$$

where e is the film thickness and P_0 the saturation vapor pressure of water at room temperature.

2.4.5. Tensile tests

Uniaxial tensile tests were carried out in an Instron dynamometer at a crosshead speed of 1.2 mm/min at room temperature, following ASTM D882-02 (2002) standard recommendation. Nominal stress (σ)–strain (ε) curves were obtained and Young's modulus (E), tensile strength (σ_u), strain at break (ε_b) and tensile toughness values were determined.

3. Results and discussion

3.1. Morphological characterization

Fig. 2a and b shows the images acquired by optical microscopy of the films produced with 0.02 wt.% of NHF and with the same content of commercial carbon nanotubes, respectively. The figures clearly show that while the film containing NHF did not show the presence of aggregates, these are clearly visible in the film prepared with commercial carbon nanotubes (see, for example, the areas marked with circles in Fig. 2b).

The cryogenic fracture surface micrographs of the matrix and composites NHF-0.02, NHF-0.04 and NHF-0.10 are shown from Fig. 2c–f, respectively. The matrix displays a fracture surface with prominent raised features, known as hackle bands, which are attributed to craze formation and propagation (Wolock, Newman, & Kies, 1959). In contrast the fracture surface of the composites shows a well-developed vein pattern suggesting a ductile yielding. The yielding phenomenon of polymers is highly time and temperature dependent, with the competition between shear and dilatational yielding integrally linked to the local stress state of each volume element in the material. Therefore, a transition from brittle-to-ductile behavior can occur if the stress state in the polymer is changed in such a way that the shear yield criterion is reached prior to the formation of crazes (i.e., homogeneous yielding by shear vs heterogeneous yielding by crazing) (Sternstein, 1975). Well dispersed carbon nanotubes can suppress craze formation and promote delocalized shear yielding. Then, the main crack is formed by the accumulation of the micro tearing along near shear bands and the torn shear bands form vein patterns on the fracture surface (Bian, Chen, He, & Hui, 2001). If the nanofiller remains well dispersed, an increment in its concentration would lead to a thinner and denser pattern of veins as reported by Bian, He, and Chen (2002). Instead of this trend, the cryogenic fracture surface of the composites with NHF progressively lose their vein structure as

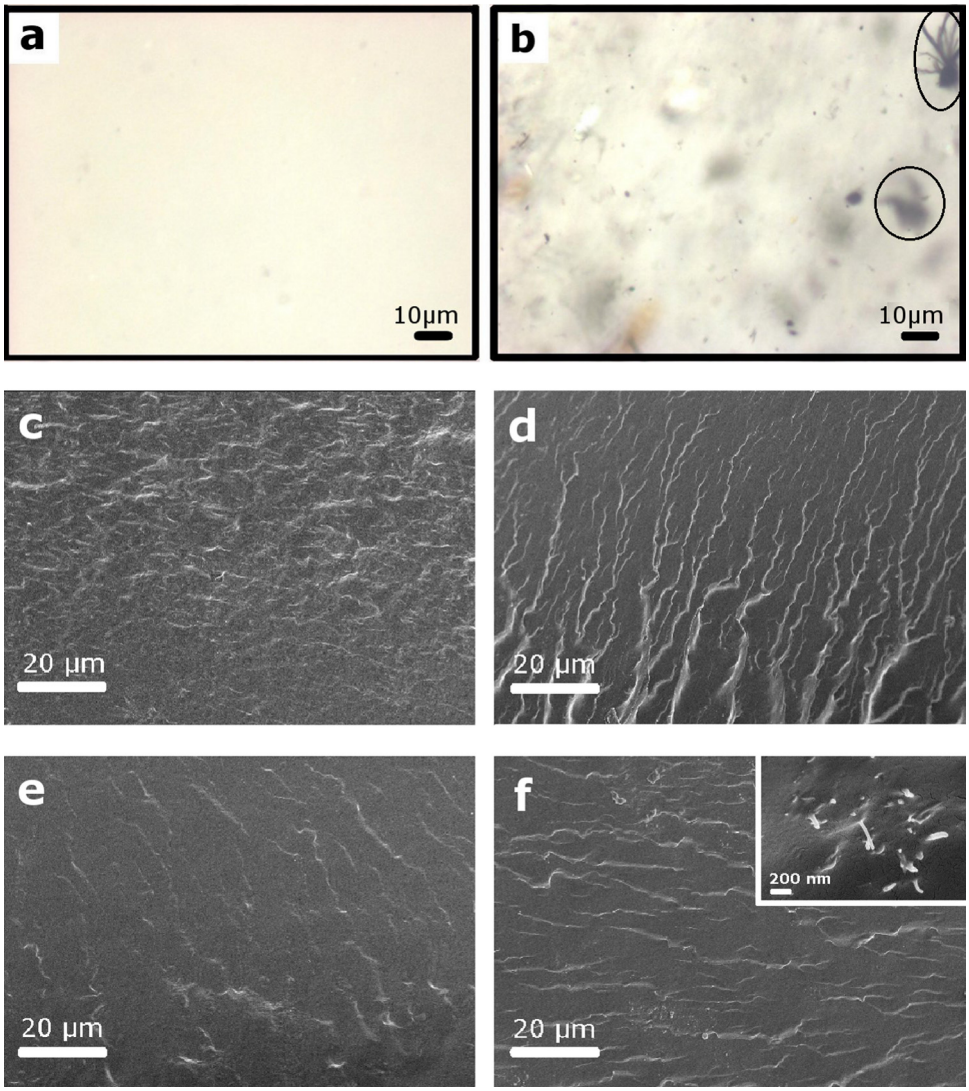

Fig. 2. Optical microscopy of composites: (a) NHF-0.02 and (b) 0.02 wt.% commercial MWCNT. FE-SEM micrograph of cryogenic fracture surface of: (c) matrix, (d) NHF-0.02, (e) NHF-0.04, (f) NHF-0.10. The inset in (f) shows areas with aggregates of NHF.

the nanofiller content increases, suggesting that the NHF begins to agglomerate.

All of these results indicate that the hybrid is much better dispersed within the matrix than commercial MWCNT. The physicochemical phenomenon related causing the higher dispersibility of the NHF in water may also be operating during starch gelatinization, but loses effectiveness when the nanofiller content increases.

3.2. Crystallinity of nanocomposites

Fig. 3 shows the X-ray diffraction patterns of nano-hybrid filler, matrix and all the composites. The starch crystallite size obtained by the Scherrer equation (Patterson, 1939) and the starch crystalline fraction (C.F) calculated according to Famá, Flores, Gerschenson, and Goyanes (2006) are also included. The diffraction pattern obtained for NHF was added as a reference (Fig. 3a). This pattern exhibits typical features of carbon nanotubes ($2\theta = 26^\circ$) and the most intense hercynite peak ($2\theta = 31^\circ$). The XRD pattern of the matrix (Fig. 3b) shows three peaks at $2\theta = 14^\circ$, 17° and 19.8° which are characteristic of the B-type crystalline structure (Buléon, Véronèse, & Putaux, 2007). Two small peaks appear at $2\theta = 13^\circ$ and 20.2° (a shoulder at the right side of the peak at 19.8°) as first indicators that a hydrated V-type structure is being formed by the amylose fraction as a result of its complexation with glycerol. The small crystalline fraction displayed by the matrix (3.9%) is a consequence of the retrogradation process resulting from the four week storage at 57.5% RH. This well known behavior was previously reported by other authors (Farhat et al., 2000; Van Soest, de Wit, Tournois, & Vliegenthart, 1994; Wynne-Jones & Blanshard, 1986).XRD patterns of NHF-0.02, NHF-0.04 and NHF-0.10 (Fig. 3c–e), show that the addition of NHF has no influence on the crystalline structure but increases the crystalline fraction of the films. The addition of the hybrid notably increases the intensity of the $2\theta = 14^\circ$ and 17° diffraction peaks with respect to these peaks in the matrix. Interestingly, the highest intensity is obtained with the lowest percentage of filler used in this work. This result suggests that higher percentages of filler lead to a diminution of the intensity of both peaks with respect to the NHF-0.02 film, being more apparent when $2\theta = 17^\circ$. The crystallite size, as the crystalline fraction, follows the same trend with NHF content. The peaks at $2\theta = 13^\circ$, 19.8° and 20.2° are not modified suggesting that the complexation of glycerol with amylose is not involved in this phenomena.

The XRD pattern of the films was modeled using the March–Dollase model (Dollase, 1986; March, 1932) in the Powder Cell program (Kraus & Nolze, 1996). The XRD pattern of the matrix was modeled assuming a random distribution of crystallites, but

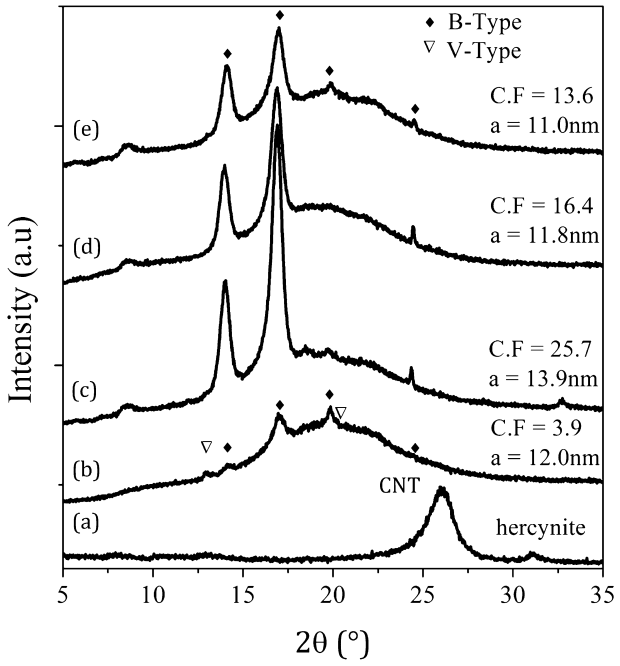

Fig. 3. X-ray diffractions patterns for: (a) nano-hybrid filler, (b) matrix, (c) NHF-0.02, (d) NHF-0.04 and (e) NHF-0.10.

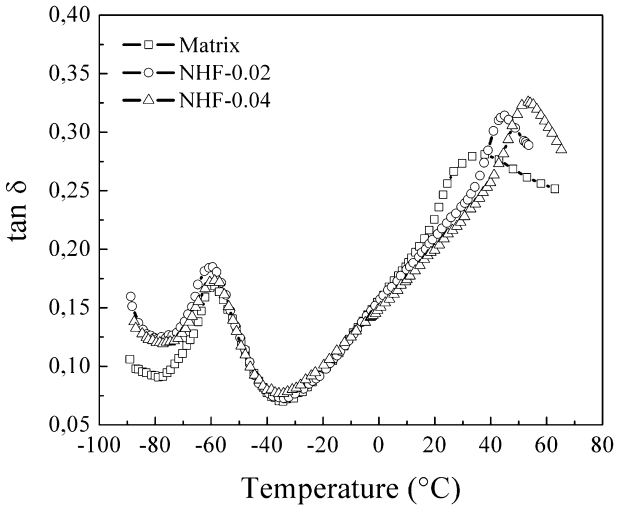

Fig. 4. Evolution of tanδ as a function of temperature for matrix and composites.

under the same hypothesis it was not possible to model the XRD patterns of the composites. The high intensities of the peaks at $2\theta = 14^\circ$ and 17° observed in the composite films, corresponding to the planes (2 0 1) and (2 1 1) of the B-type structure, can be modeled considering that the crystallites take the form of platelets with a perfect alignment of the ⟨4 1 2⟩ direction with the normal of the film. These results indicate that the incorporation of the NHF to the starch glycerol matrix leads to the growing of the crystallite in a preferential orientation.

It is well known that the presence of nanoparticles in a polymeric matrix may modify the crystallization behavior acting as nucleation centers (Angles & Dufresne, 2000). For instance, Wu and Chen (2006) studied the effect of MWCNTs on the crystallization of poly(ε-caprolactone) (PCL) finding that the filler induces two opposite effects. At low MWCNT contents the filler acts as a nucleating agent, accelerating the crystallization of the polymer. In contrast, higher MWCNT contents hinder the transport of polymer segments delaying the crystallization process. Their results indicate that the addition of MWCNTs into PCL induces the heterogeneous nucleation at lower MWCNT content and then reduces the transportation ability of polymer chains during crystallization processes at higher MWCNT content.

On the other hand, Angles and Dufresne (2000) showed that in starch–cellulose whiskers composites there is a selective migration of the plasticizer from the matrix through the whisker/matrix interface as consequence of the higher affinity between cellulose whiskers and plasticizer. Based on the high dispersibility of the NHF in polar solvents (Morales et al., 2013), high affinity between the NHF and the glycerol is expected. This interaction may be supported by the formation of hydrogen bonding between the hydroxylated surface of the ceramic oxide nanoparticles (forming part of the NHF) and the hydroxyl groups of glycerol. Additionally Forssell et al. (1997) showed that glycerol interacts with starch, inhibiting the amylopectin crystallization. Then, the higher the glycerol content in the starch matrix the lower the crystallinity of the system (Farahnaky et al., 2013; Van Soest et al., 1994; Van Soest, de Wit, Tournois, & Vliegenthart, 1996).

The previous statements help to interpret the results of Fig. 3. At low content of NHF two simultaneous effects lead to an increment of the crystalline fraction. On one hand, as explained by Wu and Chen (2006), the NHF may act as nucleation centers triggering crystallization. On the other hand, due to the migration of glycerol from the matrix to the NHF/matrix interface, the content of plasticizer in the matrix acts against amylopectin crystallization. At high NHF content a diminution in the crystalline fraction with increasing content of filler could be a consequence of steric hindering produced by the NHF. High content of NHF may lead to an entangled structure that reduces the mobility of amorphous amylopectin chains, limiting crystallization. The observed reduction in crystallite size with increasing NHF is consistent with the last explanation.

3.3. Thermal characterization

The evolution of tanδ as a function of temperature for matrix and composites is shown in Fig. 4. Starch plasticized with glycerol behaves as a partially miscible system with two main relaxation phenomena evidenced through two maxima in tanδ curves. The low temperature relaxation occurs around −60 °C and is attributed to the glass transition of the glycerol-rich phase (T_g^α) whereas the high temperature relaxation at 37 °C corresponds to the glass transition of starch-rich domains (T_g^β). Both relaxation temperatures are reported in Table 2. The T_g^α value is not influenced whereas T_g^β significantly increases upon NHF addition.

Fig. 5 shows the thermogravimetric curves of the matrix and all the different composites. The TGA curve of matrix shows an initial mass drop of approximately 12 wt.% in the range 35–150 °C which corresponds to the loss of absorbed moisture, according to Angles and Dufresne (2000). Then, two other losses of mass were detected which correspond to degradation processes of: (i) 150–280 °C: glycerol-rich phase and (ii) 280–350 °C: starch-rich phase (García et al., 2009; Liu, Zhao, Chen, & Yu, 2011).

Table 2
Glass transition temperatures of the matrix and composites.

	T_g^α (°C)	T_g^β (°C)
Matrix	−59 ± 1	37 ± 1
NHF-0.02	−60 ± 1	45 ± 1
NHF-0.04	−59 ± 1	53 ± 1
NHF-0.10	−59 ± 1	55 ± 1

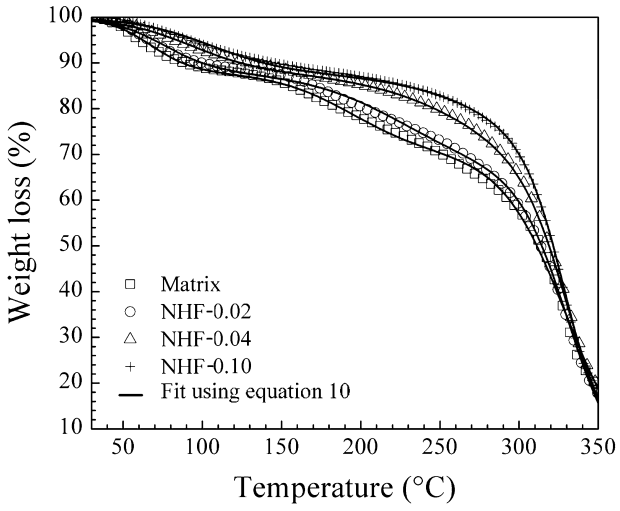

Fig. 5. Thermogravimetric curves of the matrix and composites. The solid line (–) is the theorical fit curve obtained, for each sample, using Eq. (10) and the parameter values of Table 3.

In order to discern the effect of NHF on the degradation processes of both phases (glycerol rich and starch rich phases) it would be useful to assess the kinetic parameters that govern these phenomena. To achieve this objective we have to estimate the mass fraction of the two phases in each composite. Our hypothesis is that the moisture content of each composites (12 wt.% in the conditioned sample, as indicated in Table 1) is partitioned between the alpha and beta phases, keeping the starch/water ratio constant in each phase. This hypothesis is based on the water/glycerol/starch system phase diagram reported by Godbillot et al. (2006); details about this hypothesis can be found in the Supplementary data section. Then, the composition in each phase might be described by

$$x^i_{gl} + x^i_{sw} = 1 \quad \text{with} \quad i = \alpha, \beta \tag{2}$$

where x^i_{gl} = mass fraction of glycerol in the i phase and x^i_{sw} = mass fraction of starch plus water (where the water is homogeneously dispersed in the starch matrix) in the i phase. Now, the mass fractions x^i_{gl} and x^i_{sw} can be calculated by the Gordon-Taylor equation (Kalichevsky, Jaroszkiewicz, & Blanshard, 1993; Ross & Karel, 1991), or by the Fox equation (3), a simplification that applies when the density of components is similar (Brekner, Schneider, & Cantow, 1988) (see Supplementary data for more details):

$$\frac{1}{T^i_g} = \frac{x^i_{gl}}{T^{gl}_g} + \frac{x^i_{sw}}{T^{sw}_g} \tag{3}$$

along with Eq. (2) and the values of T^i_g from Table 2 if the values of T^{gl}_g and T^{sw}_g are known. A good value for the glass transition temperature of glycerol can be easily obtained from literature, $T^{gl}_g = -90$ °C (Sou, Nishikawa, Koga, & Tozaki, 2011). To estimate T^{sw}_g our analysis is as follows. Given the initial mass of native starch (5 g) and glycerol (1.5 g), the mass of water for a starch moisture of 12% is obtained from

$$m_{total} = m_{starch} + m_{glycerol} + m_{water}$$
$$= m_{starch} + m_{glycerol} + 0.12 * m_{total} \Rightarrow m_{water} = 0.886g$$

which means that the starch plus water component has a moisture of 15%, and its glass transition temperature taken from literature is $T^{sw}_g = 60$ °C (Perdomo et al., 2009). Once the values of x^i_{gl} and x^i_{sw} were calculated, the equations of mass conservation were introduced and solved for

$$m^\alpha_{wet} = \frac{m_{glycerol}x^\beta_{sw} + (m_{starch} + m_{water})x^\beta_{gl}}{x^\alpha_{gl}x^\beta_{sw} - x^\beta_{gl}x^\alpha_{sw}} \tag{4}$$

$$m^\beta_{wet} = \frac{(m_{starch} + m_{water})x^\alpha_{gl} - m_{glycerol}x^\alpha_{sw}}{x^\alpha_{gl}x^\beta_{sw} - x^\beta_{gl}x^\alpha_{sw}} \tag{5}$$

where m^α_{wet} and m^β_{wet} are used to denote the masses of the alpha and beta phases. Finally, after obtaining the wet masses (m^α_{wet} and m^β_{wet}), the mass fractions of α dry phase $\left\{x^\alpha_{dry}\right\}$ and β dry phase $\left\{x^\beta_{dry}\right\}$ would be obtained as follows:

$$m^\alpha_{sw} = m^\alpha_{wet}x^\alpha_{sw} = m^\alpha_{starch} + m^\alpha_{water} = m^\alpha_{starch}\left(1 + \frac{m^\alpha_{water}}{m^\alpha_{starch}}\right)$$
$$= m^\alpha_{starch}\left(1 + \frac{m_{water}}{m_{starch}}\right) \tag{6}$$

where the hypothesis of constant starch/water ratio in each phase is used. Then,

$$m^\alpha_{starch} = \frac{m^\alpha_{wet}x^\alpha_{sw}}{\left(1 + \left(m_{water}/m_{starch}\right)\right)} \tag{7}$$

$$m^\alpha_{water} = m^\alpha_{wet}x^\alpha_{sw}\left(1 - \frac{1}{\left(1 + \left(m_{water}/m_{starch}\right)\right)}\right) \tag{8}$$

Then, the mass fraction of the dry phase α is:

$$x^\alpha_{dry} = \frac{m^\alpha_{wet} - m^\alpha_{water}}{m_{total}} \tag{9}$$

The mass fraction of the dry phase β was similarly calculated. The results are shown in Table 3.

The degradation kinetics of each component, water, the dry alpha and beta phases can be represented by a logistic function, so the TGA curves showed in Fig. 5 may be fitted by a combination of them (Cao, Naya, Artiaga, García, & Varela, 2004).

$$Y_{(T)} = \sum\nolimits_i x_i \frac{\exp\left[\left(4v_i/x_i\right)(T_i - T)\right]}{1 + \exp\left[\left(4v_i/x_i\right)(T_i - T)\right]} \tag{10}$$

where x_i is the mass fraction of each component at the beginning of the experiment, T_i is the center of degradation temperature range, and v_i is the weight loss rate. In the fitting procedure, the values of the mass fractions were constrained to the already estimated through the analysis of the glass transition temperatures. The parameters obtained from the adjustment of the experimental data (see details in Fig. 5) by the proposed model are presented in Table 3. At increasing NHF content, the characteristic temperature T_i for water loss and for the degradation of glycerol-rich phase increases, and both weight loss rates, v_{H_2O} and v^α_{dry}, decrease. This behavior suggests a modification in the affinity between glycerol and water molecules. This modification may be consequence of the formation of hydrogen bonding between water and the —OH of the ceramic oxide nanoparticles surface that form part of NHF (the presence of OH at the hercynite surface was already reported (Morales et al., 2013). As expected, the migration of glycerol from the starch-rich domains affects mainly the weight loss rate but not the characteristic degradation temperature. It is worth noting that these results support the model proposed to explain the high crystallization at low filler content.

Table 3
Degradation parameters of the matrix and composites.

	T_{H_2O} (°C)	v_{H_2O} (%/°C) × 10^3	x^{α}_{dry} (%)	T^{α}_{dry} (°C)	v^{α}_{dry} (%/°C) × 10^3	x^{β}_{dry} (%)	T^{β}_{dry} (°C)	v^{β}_{dry} (%/°C) × 10^3
Matrix	67.4 ± 0.7	222 ± 12	18.0	194.0 ± 0.7	184 ± 4	70.0	329.5 ± 0.3	867 ± 11
NHF-0.02	76.0 ± 0.6	177 ± 6	21.8	225.2 ± 0.5	180 ± 3	66.2	330.8 ± 0.1	1043 ± 10
NHF-0.04	92.5 ± 0.5	132 ± 2	25.5	276.2 ± 0.7	175 ± 3	62.5	331.4 ± 0.2	1078 ± 15
NHF-0.10	105.0 ± 0.2	126 ± 1	26.3	304.0 ± 0.1	174 ± 1	61.1	329.0 ± 0.1	1234 ± 6

3.4. Water vapor permeability (WVP)

Fig. 6 shows the water vapor permeability (WVP) of the matrix and composites. The addition of NHF produces a strong decrease in WVP values as the filler content increases. The NHF-0.10composite has a WVP value four times lower than the matrix.

The literature describes the behavior of water vapor permeability in a polymeric matrix as dependent simultaneously on the product of water diffusivity and the partition coefficient (solubility coefficient of water in the film) (Müller, Yamashita, & Laurindo, 2008). Thus, reducing the transport of water by diffusion through a polymer (for example: incorporation of nanotubes) reduces its permeability. Furthermore, the dispersion degree of the nanoparticles within the polymer matrix is related to the resulting barrier properties. On the other hand, reducing the solubility coefficient in the film can also cause a significant reduction in the water vapor permeability. Our assumption that new glycerol-rich domains are formed as a consequence of the interactions between the NHF, glycerol and water could explain the reduction of the available hydroxyl groups to incorporate more water molecules and so cause a reduction in the water solubility coefficient of the composite films. The increasing amount of the dry alpha phase mass fraction (x^{α}_{dry}) caused by the incorporation of NHF (see Table 3) correlates well with the decreasing of the water vapor permeability in the composites.

3.5. Mechanical characterization

Fig. 7 shows typical nominal stress–strain curves obtained under quasistatic uniaxial tensile loading conditions for the matrix and the different composites investigated. All the materials exhibit nonlinear behavior until failure, which occurs without necking before fracture. A significant improvement in Young's modulus (E), as well as an enhancement in tensile strength (σ_u) values, is obtained with the increment of NHF concentration in the nanocomposites (Table 4). The strain at break (ε_b) and tensile toughness, calculated as the area under the stress–strain curves, are also fairly increased. However, the trend of improvement holds until a nanofiller addition of 0.04 wt.% nanofiller; then a leveling off appears.

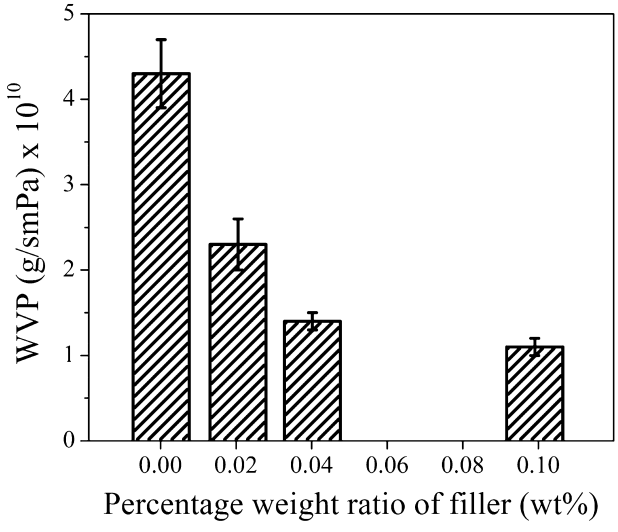

Fig. 6. WVP of matrix and composites.

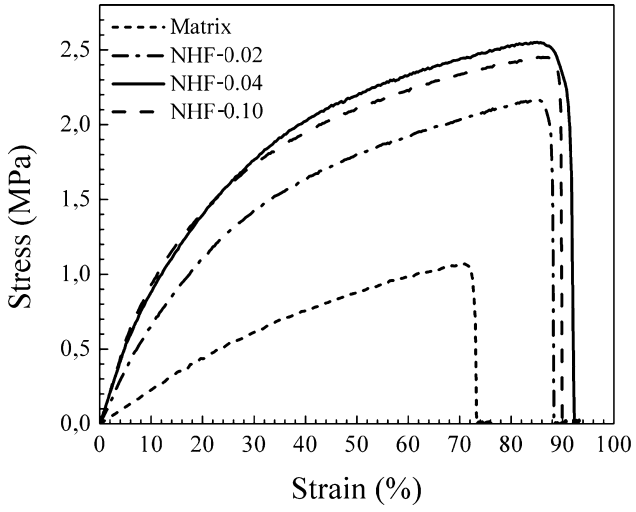

Fig. 7. Stress–strain curves for the matrix and the composites.

Table 4
Mechanical properties of the matrix and composites.

	E (MPa)	σ_u (MPa)	ε_b (%)	Tensile toughness × 10^{-6} (J/m^3)
Matrix	2.3 ± 0.1	1.07 ± 0.05	73 ± 3	0.48 ± 0.05
NHF-0.02	7.4 ± 0.1	2.17 ± 0.05	88 ± 3	1.35 ± 0.05
NHF-0.04	10.8 ± 0.1	2.55 ± 0.05	92 ± 3	1.73 ± 0.05
NHF-010	11.0 ± 0.1	2.45 ± 0.05	90 ± 3	1.64 ± 0.05

The overall mechanical behavior displayed by these composites is consistent with the characterization of the structure of its components made in previous sections. Crystallites of amylopectin B-type together with MWCNTs within the matrix increase the strength of the composite. Besides, the hercynite nanoparticles anchored to the nanotube wall ensure the stress transfer between the filler and the matrix improving its toughness. At the high filler content (0.1 wt.%), the incipient agglomeration reduces these synergistic actions and the mechanical properties deterioration begins.

4. Conclusions

This research reports structure, thermal and mechanical properties, and water vapor permeability, of a nanocomposite materials obtained from glycerol plasticized cassava starch as the matrix and a suspension of MWCNT–hercynite hybrid as a model reinforcing phase. The water dispersion of the nano-hybrid filler was obtained by simple mixing of the components, without physical/chemical functionalization or surfactants addition. The NHF has this property as consequence of its relatively low isoelectric point.

Significant changes occur in the composite systems when the NHF is homogeneously dispersed in the matrix. The analysis of the results suggests that a selective partitioning of both plasticizers

(glycerol and water) within the matrix around the hybrid occurs. A migration of the plasticizers from the amylopectin-rich domains toward the filler results and so, new glycerol-rich domains may be created in the neighborhood of the filler/matrix interface. This hinders the molecular mobility of amorphous amylopectin chains inside of the depleted amylopectin-rich domains and induces crystallization. The formation of these new glycerol-rich domains reduces the amount of hydroxyl groups available for the incorporation of more water molecules causing a reduction in the water solubility coefficient and the concomitant decreasing of water vapor permeability of the composite films. This inherent higher affinity between glycerol and water molecules induced by the NHF surface accounts for the increase of the water loss temperature and the degradation temperature of glycerol-rich domains, as well as the decrease of both weight loss rates. Finally, the internal structure of the composite material provides excellent mechanical properties with high values of Young modulus, stress at break and toughness showing the potentiality of this material in the packaging industry.

Acknowledgements

The authors wish to acknowledge the support and collaboration of the following organizations: UBA (UBACYT 2011–2014 No: 20020100100350 and UBACYT 2014–2017: 20020130100495BA); CONICET (PIP 2013–2015 11220120100508CO) and FONCyT (PICT 2012 No: 1093).

Appendix A. Supplementary data

Supplementary data associated with this article can be found, in the online version, at http://dx.doi.org/10.1016/j.carbpol.2015.03.071.

References

Angles, M. N., & Dufresne, A. (2000). Plasticized starch/tunicin whiskers nanocomposites. 1. Structural analysis. *Macromolecules*, *33*(22), 8344–8353.
Antoniou, J., Liu, F., Majeed, H., Qazi, H. J., & Zhong, F. (2014). Physicochemical and thermomechanical characterization of tara gum edible films: Effect of polyols as plasticizers. *Carbohydrate Polymers*, *111*, 359–365.
ASTM D882-02. (2002). *Annual book of ASTM*. West Conshohocken, USA: American Society for Testing and Materials.
ASTM E96-00. (2000). *Annual book of ASTM*. Philadelphia, USA: American Society for Testing and Materials.
Bian, Z., Chen, G. L., He, G., & Hui, X. D. (2001). Microstructure and ductile–brittle transition of as-cast Zr-based bulk glass alloys under compressive testing. *Materials Science and Engineering A*, *316*(1–2), 135–144.
Bian, Z., He, G., & Chen, G. L. (2002). Investigation of shear bands under compressive testing for Zr-base bulk metallic glasses containing nanocrystals. *Scripta Materialia*, *46*, 407–412.
Brekner, M.-J., Schneider, H. A., & Cantow, H.-J. (1988). Approach to the composition dependence of the glass transition temperature of compatible polymer blends: 1. *Polymer*, *29*, 78–85.
Buléon, A., Véronèse, G., & Putaux, J.-L. (2007). Self-association and crystallization of amylose. *Australian Journal of Chemistry*, *60*, 706–718.
Cao, R., Naya, S., Artiaga, R., García, A., & Varela, A. (2004). Logistic approach to polymer degradation in dynamic TGA. *Polymer Degradation and Stability*, *85*(1), 667–674.
Carvalho, A. J. F. (2011). Starch as source of polymeric materials. In S. Kalia, & L. Avérous (Eds.), *Biopolymers: Biomédical and environmental applications* (pp. 81–98). Massachusetts: Scrivener Publishing LLC.
Chang, P. R., Wu, D., Anderson, D. P., & Ma, X. (2012). Nanocomposites based on plasticized starch and rectorite clay: Structure and properties. *Carbohydrate Polymers*, *89*(2), 687–693.
Dollase, W. A. (1986). Correction of intensities for preferred orientation in powder diffractometry: Application of the March model. *Journal of Applied Crystallography*, *19*, 267–272.
Escobar, M., Goyanes, S., Corcuera, M. A., Eceiza, A., Mondragon, I., Rubiolo, G. H., et al. (2009). Purification and functionalization of carbon nanotubes by classical and advanced oxidation processes. *Journal of Nanoscience and Nanotechnology*, *9*(10), 6228–6233.
Famá, L., Flores, S. K., Gerschenson, L., & Goyanes, S. (2006). Physical characterization of cassava starch biofilms with special reference to dynamic mechanical properties at low temperatures. *Carbohydrate Polymers*, *66*(1), 8–15.
Famá, L. M., Pettarin, V., Goyanes, S. N., & Bernal, C. R. (2011). Starch/multi-walled carbon nanotubes composites with improved mechanical properties. *Carbohydrate Polymers*, *83*(3), 1226–1231.
Famá, L., Rojo, P. G., Bernal, C., & Goyanes, S. (2012). Biodegradable starch based nanocomposites with low water vapor permeability and high storage modulus. *Carbohydrate Polymers*, *87*, 1989–1993.
Farahnaky, A., Saberi, B., & Majzoobi, M. (2013). Effect of glycerol on physical and mechanical properties of wheat starch edible films. *Journal of Texture Studies*, *44*, 176–186.
Farhat, I. A., Blanshard, J. M. V., & Mitchell, J. R. (2000). The retrogradation of waxy maize starch extrudates: Effects of storage temperature and water content. *Biopolymers*, *53*, 411–422.
Forssell, P. M., Mikkilä, J. M., Moates, G. K., & Parker, R. (1997). Phase and glass transition behaviour of concentrated barley starch–glycerol–water mixtures, a model for thermoplastic starch. *Carbohydrate Polymers*, *34*, 275–282.
García, N. L., Famá, L., Dufresne, A., Aranguren, M., & Goyanes, S. (2009). A comparison between the physico-chemical properties of tuber and cereal starches. *Food Research International*, *42*, 976–982.
García, N. L., Ribba, L., Dufresne, A., Aranguren, M., & Goyanes, S. (2011). Effect of glycerol on the morphology of nanocomposites made from thermoplastic starch and starch nanocrystals. *Carbohydrate Polymers*, *84*, 203–210.
Godbillot, L., Dole, P., Joly, C., Rogé, B., & Mathlouthi, M. (2006). Analysis of water binding in starch plasticized films. *Food Chemistry*, *96*, 380–386.
Goyanes, S., Rubiolo, G. R., Salazar, A., Jimeno, A., Corcuera, M. A., & Mondragon, I. (2007). Carboxylation treatment of multiwalled carbon nanotubes monitored by infrared and ultraviolet spectroscopies and scanning probe microscopy. *Diamond and Related Materials*, *16*(2), 412–417.
Hansen, N. M. L., & Plackett, D. (2008). Sustainable films and coatings from hemicelluloses: A review. *Biomacromolecules*, *9*(6), 1493–1505.
Kalichevsky, M. T., & Blanshard, J. M. V. (1992). A study of the effect of water on the glass transition of 1:1 mixtures of amylopectin, casein and gluten using DSC and DMTA. *Carbohydrate Polymers*, *19*, 271–278.
Kalichevsky, M. T., Jaroszkiewicz, E. M., Ablett, S., Blanshard, J. M. V., & Lillford, P. J. (1992). The glass transition of amylopectin measured by DSC, DMTA and NMR. *Carbohydrate Polymers*, *18*, 77–88.
Kalichevsky, M. T., Jaroszkiewicz, E. M., & Blanshard, J. M. V. (1993). A study of the glass transition of amylopectin–sugar mixtures. *Polymer*, *34*(2), 346–358.
Kong, Y., Yuan, J., & Qiu, J. (2012). Preparation and characterization of aligned carbon nanotubes/polylactic acid composite fibers. *Physica B: Condensed Matter*, *407*(13), 2451–2457.
Kraus, W., & Nolze, G. (1996). POWDER CELL—A program for the representation and manipulation of crystal structures and calculation of the resulting X-ray powder patterns. *Journal of Applied Crystallography*, *29*, 301–303.
Kudus, M. H. A., Akil, H. M., Mohamad, H., & Loon, L. E. (2011). Effect of catalyst calcination temperature on the synthesis of MWCNT–alumina hybrid compound using methane decomposition method. *Journal of Alloys and Compounds*, *509*(6), 2784–2788.
Liu, Z., Zhao, L., Chen, M., & Yu, J. (2011). Effect of carboxylate multi-walled carbon nanotubes on the performance of thermoplastic starch nanocomposites. *Carbohydrate Polymers*, *83*(2), 447–451.
March, A. (1932). Matematischetheorie des regelungnach der korngestaltbeiaffiner deformation. *Zeitschriftfür Kristallographie*, *81*, 285–297.
Moates, G. K., Noel, T. R., Parker, R., & Ring, S. G. (2001). Dynamic mechanical and dielectric characterisation of amylose glycerol films. *Carbohydrate Polymers*, *44*, 247–253.
Morales Mendoza, N., Goyanes, S., Chiliotte, C., Bekeris, V., Rubiolo, G., & Candal, R. (2012). Magnetic binary nanofillers. *Physica B: Condensed Matter*, *407*(16), 3203–3205.
Morales, N. J., Goyanes, S., Chiliotte, C., Bekeris, V., Candal, R. J., & Rubiolo, G. H. (2013). One-step chemical vapor deposition synthesis of magnetic CNT–hercynite ($FeAl_2O_4$) hybrids with good aqueous colloidal stability. *Carbon*, *61*, 515–524.
Müller, C. M. O., Yamashita, F., & Laurindo, J. B. (2008). Evaluation of the effects of glycerol and sorbitol concentration and water activity on the water barrier properties of cassava starch films through a solubility approach. *Carbohydrate Polymers*, *72*(1), 82–87.
Nafchi, A. M., Alias, A. K., Mahmud, S., & Robal, M. (2012). Antimicrobial, rheological, and physicochemical properties of sago starch films filled with nanorod-rich zinc oxide. *Journal of Food Engineering*, *113*(4), 511–519.
Nuanmano, S., Prodpran, T., & Benjakul, S. (2015). Potential use of gelatin hydrolysate as plasticizer in fish myofibrillar protein film. *Food Hydrocolloids*, *47*, 61–68.
Patterson, A. L. (1939). The scherrer formula for X-ray particle size determination. *Physical Review*, *56*, 978–982.
Perdomo, J., Cova, A., Sandoval, A. J., García, L., Laredo, E., & Müller, A. J. (2009). Glass transition temperatures and water sorption isotherms of cassava starch. *Carbohydrate Polymers*, *76*(2), 305–313.
Prasad, K. E., Das, B., Maitra, U., Ramamurty, U., & Rao, C. N. R. (2009). Extraordinary synergy in the mechanical properties of polymer matrix composites reinforced with 2 nanocarbons. *Proceedings of the National Academy of Sciences of the United States of America*, *106*(32), 13186–13189.
Ross, Y., & Karel, M. (1991). Water and molecular weight effects on glass transitions in amorphous carbohydrates and carbohydrate solutions. *Journal of Food Science*, *56*, 1676–1681.
Schmitt, H., Prashantha, K., Soulestin, J., Lacrampe, M. F., & Krawczak, P. (2012). Preparation and properties of novel melt-blended halloysite nanotubes/wheat starch nanocomposites. *Carbohydrate Polymers*, *89*(3), 920–927.

Sou, K., Nishikawa, K., Koga, Y., & Tozaki, K. (2011). High-resolution calorimetry on thermal behavior of glycerol (I): Glass transition, crystallization and melting, and discovery of a solid–solid transition. *Chemical Physics Letters*, *506*(4–6), 217–220.

Sternstein, S. S. (1975). Yielding in glassy polymers. In *American society for metals: Polymeric materials: Relationships between structure and mechanical behavior*. Ohio: American Society for Metal Metals Park.

Sun, D., Chu, C.-C., & Sue, H.-J. (2010). Simple approach for preparation of epoxy hybrid nanocomposites based on carbon nanotubes and a model clay. *Chemistry of Materials*, *22*(12), 3773–3778.

Swain, S. K., Pradhan, A. K., & Sahu, H. S. (2013). Synthesis of gas barrier starch by dispersion of functionalized multiwalled carbon nanotubes. *Carbohydrate Polymers*, *94*(1), 663–668.

Tian, F., & He, C. N. (2011). Processing and mechanical properties of carbon nanotube–alumina hybrid reinforced high density polyethylene composites. *Materials Research Bulletin*, *46*(7), 1143–1147.

Van Soest, J. J. G., de Wit, D., Tournois, H., & Vliegenthart, J. F. G. (1994). The influence of glycerol on structural changes in waxy maize starch as studied by Fourier transform infra-red spectroscopy. *Polymer*, *35*(22), 4722–4727.

Van Soest, J. J. G., Hulleman, S. H. D., de Wit, D., & Vliegenthart, J. F. G. (1996). Crystallinity in starch bioplastics. *Industrial Crops and Products*, *5*, 11–22.

Wilhelm, H. M., Sierakowski, M. R., Souza, G. P., & Wypych, F. (2003). Starch films reinforced with mineral clay. *Carbohydrate Polymers*, *52*, 101–110.

Wolock, I., Newman, S. B., & Kies, J. A. (1959). Fracture phenomena in polymers. In B. L. Averbach, D. K. Felbeck, G. T. Hahn, & D. A. Thomas (Eds.), *Fracture: Proceedings of an international conference on the atomic mechanisms of fracture* (pp. 250–264). New York, NY: John Wiley and Sons Inc.

Wu, T. M., & Chen, E. C. (2006). Isothermal and nonisothermal crystallization kinetics of poly(ε-caprolactone)/multi-walled carbon nanotube composites. *Polymer Engineering & Science*, *46*(19), 1309–1317.

Wynne-Jones, S., & Blanshard, J. M. V. (1986). Hydration studies of wheat starch, amylopectin, amylose gels and bread by proton magnetic resonance. *Carbohydrate Polymers*, *6*, 289–306.

Zilli, D., Goyanes, S., Escobar, M. M., Chiliotte, C., Bekeris, V., Cukierman, A. L., et al. (2007). Comparative analysis of electric, magnetic, and mechanical properties of epoxy matrix composites with different contents of multiple walled carbon nanotubes. *Polymer Composites*, *28*(5), 612–617.